RESEARCH ARTICLE | APRIL 01 2000

The $c\,^3\Sigma^+$, $b\,^3\Pi$, and $a\,^3\Sigma^+$ states of NaK revisited

R. Ferber; E. A. Pazyuk; A. V. Stolyarov; ... et. al

J. Chem. Phys. 112, 5740–5750 (2000)
https://doi.org/10.1063/1.481149

The $c\ ^3\Sigma^+$, $b\ ^3\Pi$, and $a\ ^3\Sigma^+$ states of NaK revisited

R. Ferber
Department of Physics, University of Latvia, Riga LV-1586, Latvia

E. A. Pazyuk, A. V. Stolyarov, and A. Zaitsevskii
Department of Chemistry, Moscow State University, Moscow, 119899, Russia

P. Kowalczyk
Institute of Experimental Physics, Warsaw University, ul. Hoza 69, 00-681 Warsaw, Poland

Hongmin Chen, He Wang, and William C. Stwalley
Department of Physics, Department of Chemistry, and Institute of Material Science, University of Connecticut, Storrs, Connecticut 06269-3046

(Received 2 November 1999; accepted 4 January 2000)

We present new $c\ ^3\Sigma^+ \rightarrow a\ ^3\Sigma^+$ laser induced fluorescence spectra of the NaK molecule, which clearly indicate that $v_0=20$ is the first vibrational level of the $c\ ^3\Sigma^+$ state lying above $v=0$ of $B\ ^1\Pi$ state. These spectra are used in a multistep deperturbation ($B\ ^1\Pi \sim c\ ^3\Sigma^+ \sim b\ ^3\Pi$) procedure to obtain improved $a\ ^3\Sigma^+$, $b\ ^3\Pi$ and $c\ ^3\Sigma^+$ potential energy curves. The deperturbation analysis is confirmed by the calculated electronic $B\ ^1\Pi \sim c\ ^3\Sigma^+$ and $c\ ^3\Sigma^+ \sim b\ ^3\Pi$ spin–orbit matrix elements obtained from many-body multipartitioning perturbation theory employing the relativistic effective potential method. © *2000 American Institute of Physics*. [S0021-9606(00)00213-0]

I. INTRODUCTION

NaK is presently the best understood heteronuclear alkali dimer, being the test molecule for spectroscopic studies in the visible range. For a number of electronic states high quality *ab initio* calculations exist[1–8] that are not available for other heteronuclear alkali diatomics. Such species are now of increased interest because of studies of collision dynamics and photoassociative spectra involving laser cooled and trapped alkaline atoms.

Low lying triplet states of NaK have been studied extensively during recent years with a wide variety of high resolution, perturbation facilitated laser spectroscopy techniques. Detailed information about the lowest $a\ ^3\Sigma^+$ state correlating to the first atomic asymptote, $\mathrm{Na}(3s)+\mathrm{K}(4s)$, as well as about the $b\ ^3\Pi$ and $c\ ^3\Sigma^+$ states correlating to the second dissociation limits $\mathrm{Na}(3s)+\mathrm{K}(4p)$ (see Fig. 1), is important since these states can be used to investigate higher triplet states in multistep optical excitation and stimulated emission experiments. In spite of considerable work on the $a\ ^3\Sigma^+$,[9–13] $b\ ^3\Pi$,[14,15] and $c\ ^3\Sigma^+$ (Refs. 16–23) states of NaK, a number of unresolved questions about them still remains.

One of the problems not yet solved properly was the lack of data on low vibrational levels of the $c\ ^3\Sigma^+$ state which was the reason for the ambiguous vibrational numbering of levels in this state. In particular, for levels with v less than v_0, which is the first $c\ ^3\Sigma^+$ state level above $v=0$ of the $B\ ^1\Pi$ state, there are no near degenerate singlet levels from which intensity can be borrowed. As a result, various v_0 values as 20,[12,16] 16,[17,18] and 12 (Ref. 20) have been proposed by different assignment methods. Derouard and Sadeghi[16] used $e-f$ Stark mixing spectroscopy to locate 50 centers of $B\ ^1\Pi \sim c\ ^3\Sigma^+$ perturbation attributed to 21 different vibrational levels of the $c\ ^3\Sigma^+$ state and thus determined effective molecular constants as parametric functions of the v_0 level. A comparison with theoretical calculations of Stevens, Konowalow, and Ratcliff[2] yielded $v_0=20\pm2$. In succeeding works[17,18] vibrational assignment was performed by the perturbation matrix element method.[24] Observation of the vibrational variation of spin–orbit perturbation matrix elements led to $v_0=16\pm1$.[17] In the work[18] the fragments of $B\ ^1\Pi - X^1\Sigma^+$ system perturbed by the $c\ ^3\Sigma^+$ state were observed for different isotopes ^{23}Na ^{39}K and ^{23}Na ^{41}K. It turned out however that the attempt to establish absolute $c\ ^3\Sigma^+$ state vibrational numbering from isotopic shifts produced inconclusive results. When the lowest sampled vibrational level of the perturbation exceeds 10, this method is not more reliable than the matrix element method.[24] In the meantime Katô and co-workers performed several experiments on the same perturbed system,[19–23] assigning $v_0=12$ from observation of the intensity pattern in the bound–bound part of the $c\ ^3\Sigma^+ \rightarrow a\ ^3\Sigma^+$ fluorescence.[20] Finally, analysis of the observed $c\ ^3\Sigma^+ - a\ ^3\Sigma^+$ emission in the bound-free part[12] suggested strongly that $v_0=20$. We attempt here to explain why different methods provide different v_0 values and, of primary importance, which one of them is correct.

On the contrary, the spectroscopic information about the low vibrational levels of the $b\ ^3\Pi$ state is reliable enough.[14] The set of molecular constants allows one to construct the RKR potential with satisfactory accuracy for the observed vibrational levels from $v=0$ to $v=49$. However, as can be seen from Fig. 1, the highest observed $b\ ^3\Pi$ level lies below the first observed $c\ ^3\Sigma^+$ level. At the same time, it is quite obvious that it is the unknown part of the $b\ ^3\Pi$ term that is responsible for $c\ ^3\Sigma^+ \sim b\ ^3\Pi$ interaction. Hence, there is an acute need for extension of the $b\ ^3\Pi$ potential to higher v's.

The lowest triplet state $a\ ^3\Sigma^+$, which is mostly repulsive, but with a shallow van der Waals minimum (see Fig. 1) was extensively studied spectroscopically.[9–13] The bound

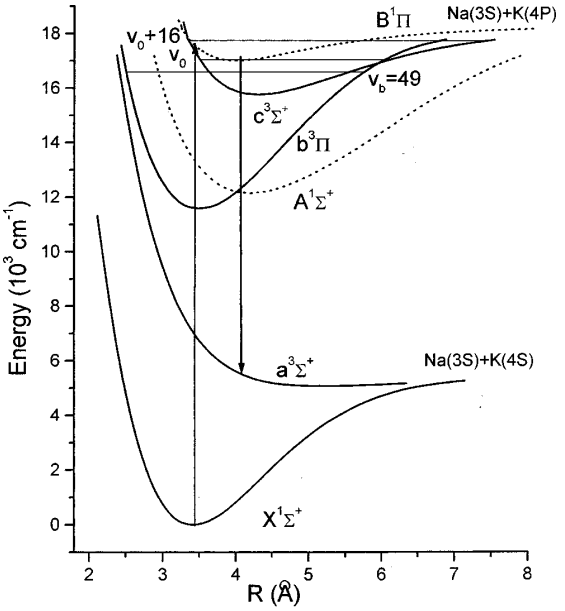

FIG. 1. NaK potential curves corresponding to the two lowest dissociation limits. The arrows show excitation to the $B\ ^1\Pi \sim c\ ^3\Sigma^+ \sim b\ ^3\Pi$ perturbed levels followed by fluorescence to the $a\ ^3\Sigma^+$ state. v_0 denotes the first vibrational level of the $c\ ^3\Sigma^+$ state lying above $v=0$ in the $B\ ^1\Pi$ state.

part of the $a\ ^3\Sigma^+$ term up to the vibrational level $v=11$ was determined in Ref. 9. Recently, vibrational levels near the dissociation limit of the $a\ ^3\Sigma^+$ state have been comprehensively investigated in Ref. 10, and the high-accuracy potential curve valid up to the last ($v_{\max}=19$) bound $a\ ^3\Sigma^+$ level was constructed by the inverse perturbation analysis (IPA) method.[25] The repulsive part of the $a\ ^3\Sigma^+$ potential has been obtained from $b\ ^3\Pi \rightarrow a\ ^3\Sigma^+$,[11] $c\ ^3\Sigma^+ \rightarrow a\ ^3\Sigma^+$,[12] and $d^3\Pi \rightarrow a\ ^3\Sigma^+$ (Ref. 13) continuum emission spectra by different inversion procedures. However, since bound and repulsive parts of the $a\ ^3\Sigma^+$ state were studied in different spectral regions, the behavior of the potential in the junction region was less well studied.

The main goal of the present paper was to perform unambiguous vibrational assignment of the $c\ ^3\Sigma^+$ state by remeasuring $c\ ^3\Sigma^+ \rightarrow a\ ^3\Sigma^+$ fluorescence intensity pattern, as well as by reprocessing the existing high accuracy data for $B\ ^1\Pi \sim c\ ^3\Sigma^+ \sim b\ ^3\Pi$ complex, and, as a result, to obtain improved $c\ ^3\Sigma^+$, $b\ ^3\Pi$, and $a\ ^3\Sigma^+$ potentials. The paper is structured as follows. Section II describes LIF experiments resulting in the intensity pattern of the bound–bound and partially bound-free $c\ ^3\Sigma^+ \rightarrow a\ ^3\Sigma^+$ spectra. Section III describes electronic structure calculation of the spin–orbit interaction parameters. The multistep inversion procedure used to obtain accurate RKR potential curves of the $c\ ^3\Sigma^+(v=0-36)$ and $b\ ^3\Pi(v=0-63)$ states together with the refined repulsive limb of the $a\ ^3\Sigma^+$ state is presented in Sec. IV. Nonadiabatic radiative properties of the $B\ ^1\Pi \sim c\ ^3\Sigma^+ \sim b\ ^3\Pi$ complex are simulated in Section V. It is worth mentioning that since $^3\Sigma$ states belong to almost pure Hund's case (b) coupling, both quantum numbers N and J ($J=N, N=1$) will be used by us to label a particular molecular state. The $b\ ^3\Pi$ state belongs to intermediate (a)–(b) Hund's case, but since only levels with small J are involved we will assume that case (a) is preferable and use quantum number J for this state, as well as for the singlet states.

II. $c\ ^3\Sigma^+ \rightarrow a\ ^3\Sigma^+$ LIF MEASUREMENTS

A. Experimental setup

The experimental setup and equipment used by us is typical for laser-induced fluorescence measurements. Briefly, NaK molecules were formed in heat-pipe oven containing approximately 1/4 mixture (by weight) of potassium and sodium metals. The $B\ ^1\Pi \sim c\ ^3\Sigma^+ \leftarrow X^1\Sigma^+$ transitions in the region 570–581 nm were excited by a laser beam from a single mode ring dye laser (Coherent Innova 899) using rhodamine 6G with typically 250–300 mW power. The dye laser scan and laser wavelength measurements have been accomplished using Coherent Autoscan computer storage. This system, along with wavelength calibration by an iodine absorption cell allowed us to reach accuracy and reproducibility of the order of 0.001 cm^{-1}. The $c\ ^3\Sigma^+ - a\ ^3\Sigma^+$ molecular fluorescence observed at a right angle to the incident laser beam was analyzed between 790 and 830 nm by a McPherson 270 0.35 m scanning monochromator (reciprocal dispersion 20 Å /mm with 1200 groves/mm, 48×48 mm replica, blazed at 500 nm). The spectra were recorded with a 9659 QB (S20 cathode type) photomultiplier cooled to −7.5 °C. The photoelectric current was detected by a Keithley 427 current amplifier. The spectral response of the whole detection system was checked by recording the Ti–sapphire Innova 899 Ring laser output power over the whole tuning range, by monitoring it with a laser power meter (Vector S310 Scientech). The frequency of the observed fluorescence was calibrated using neon and uranium lines from hollow cathode discharge lamps. The absolute accuracy of wave numbers in the LIF spectra is about 2–3 cm^{-1}.

B. LIF spectra

We excited selectively four strongly coupled $B\ ^1\Pi \sim c\ ^3\Sigma^+$ levels of the $^{23}Na\ ^{39}K$ molecule given in Ref. 12, namely: $B\ ^1\Pi(v=4,J^e=13) \sim c\ ^3\Sigma^+(v_0+5,N=J^e=13) \leftarrow X^1\Sigma^+(v=0,J=14)$, $\nu_{\text{laser}}=17\,220.4705$ cm^{-1}; $B\ ^1\Pi(v=6,J^f=31) \sim c\ ^3\Sigma^+(v_0+8,N=30,J^f=31) \leftarrow X^1\Sigma^+(v=0,J=31)$, $\nu_{\text{laser}}=17\,314.6890$ cm^{-1}; $B\ ^1\Pi(v=8,J^e=46) \sim c\ ^3\Sigma^+(v_0+11,N=J^e=46) \leftarrow X^1\Sigma^+(v=0,J=45)$, $\nu_{\text{laser}}=17\,388.3084$ cm^{-1}; $B\ ^1\Pi(v=10,J^f=31) \sim c\ ^3\Sigma^+ \times(v_0+13,N=30,J^f=31) \leftarrow X^1\Sigma^+(v=0,J=31)$, $\nu_{\text{laser}}=17\,515.6528$ cm^{-1}, as well as one level given in Ref. 20, namely $B\ ^1\Pi(v=10,J^f=36) \sim c\ ^3\Sigma^+(v_0+13,N=37,J^f=36) \leftarrow X^1\Sigma^+(v=0,J=36)$, $\nu_{\text{laser}}=17\,502.0853$ cm^{-1}. Here J^e, J^f refer to e,f parity of the excited rotational level. The excitation was followed by $c\ ^3\Sigma^+ \rightarrow a\ ^3\Sigma^+$ emission in the near infrared region that was recorded. The $c\ ^3\Sigma^+ \rightarrow a\ ^3\Sigma^+$ LIF spectra presented in Fig. 2(a) consist of the well-resolved bound–bound part and a fragment of the bound–free part. Rovibrational assignment of each LIF progression from all five of the above-mentioned states into all

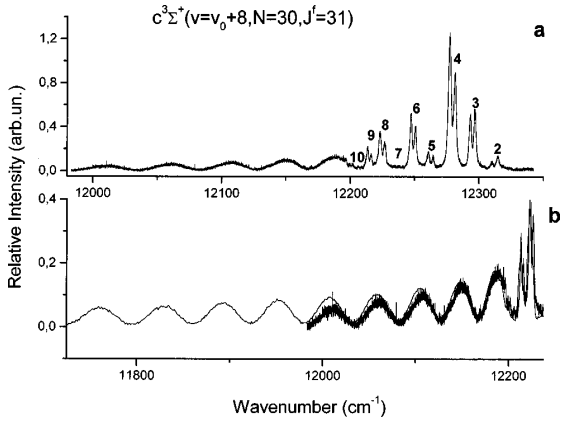

FIG. 2. (a) The bound–bound, bound–quasibound and part of bound-free $c\ ^3\Sigma^+ \rightarrow a\ ^3\Sigma^+$ emission observed experimentally after excitation of a single rovibrational level in the $c\ ^3\Sigma^+$ state. The numbers on the top of the peaks denote vibrational assignment of the $a\ ^3\Sigma^+$ state. (b) Matching of the bound–free part of the spectrum with the corresponding spectrum from Ref. 12 which extends farther to the red.

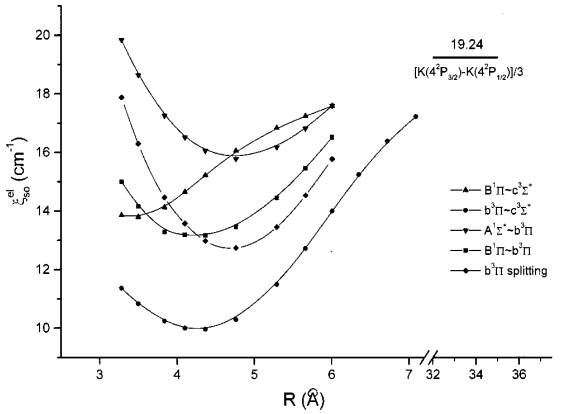

FIG. 3. Calculated electronic spin–orbit matrix elements between all singlet and triplet states correlating to the second dissociation limit of NaK, displayed as a function of internuclear distance R. $B\ ^1\Pi \sim b\ ^3\Pi$ and $b\ ^3\Pi$ splitting functions are taken from Ref. 7. The horizontal line represents the asymptotic value calculated from the experimental atomic data.

bound and quasibound $a\ ^3\Sigma^+$ states has been determined unambiguously using the refined spectroscopic constants of the $X^1\Sigma^+$ state from Ref. 26 as well as by direct numerical solution of radial Schrödinger equation[27] with the IPA potential curve for the $a\ ^3\Sigma^+$ state given in Ref. 10. Although the spectral resolution of the monochromator allowed us to achieve 2–3 cm^{-1} accuracy in line positions, this appeared to be satisfactory for unambiguous rovibrational assignment, and since our aim was to fit the intensity distribution, we had no intention to strive for any better spectral accuracy. We could recognize transitions to all bound $a\ ^3\Sigma^+$ levels up to quasi-bound levels on the border of the continuum [see Fig. 2(a)]. It was possible, for the three $c\ ^3\Sigma^+$ levels with $v=v_0+8, N=30, J^f=31$; $v=v_0+11$, $N=J^e=46$ and $v=v_0+13, N=30, J^f=31$, to compare our patterns with the calculated ones presented in Fig. 8 of Ref. 20, showing that the bound–bound $c\ ^3\Sigma^+ \rightarrow a\ ^3\Sigma^+$ LIF patterns differ dramatically. However, when we increased by one the $a\ ^3\Sigma^+$ state vibrational numbering given in Ref. 20, the patterns agreed completely with each other.

The bound–free parts of the spectra, one of which is presented in Fig. 2(a), are in full agreement with the respective spectra given in Ref. 12. This allowed us to match the obtained bound-free spectra with their counterparts from Ref. 12 in order to get the full $c\ ^3\Sigma^+ \rightarrow a\ ^3\Sigma^+$ pattern for four of the progressions. An example of such matching is given in Fig. 2(b).

III. ELECTRONIC SPIN–ORBIT COUPLING CALCULATIONS

The spin–orbit (SO) interaction parameters were calculated by the two-step quasirelativistic approach[7,28,29] which combines the description of the relativistic effects through effective core potentials (REP)[30,31] with the treatment of electronic correlations by the many-body multipartitioning perturbation theory (MPPT).[32,33] Only the inner core shells $1s^2$ for Na and $1s^22s^22p^6$ for K were replaced by REP's, leaving the 18-electron problem for explicit treatment. The scalar many-electron problem with spin-averaged REP was solved by constructing and diagonalizing the state-selective effective Hamiltonian for the valence two-electron subsystem which incorporated the core polarization and core-valence correlations at the second order of the MPPT. The SO matrix elements between resulting eigenstates were evaluated using the spin-orbit potentials from Refs. 30 and 31 uniformly scaled in order to fit the experimental atomic fine-structure splittings at the dissociation limits. The detailed description of the computational procedure can be found in Ref. 7. The computed SO matrix elements $\xi_{SO}^{el}(R)$ are presented in Fig. 3. A comparison of the calculated $A^1\Sigma^+ \sim b\ ^3\Pi$ and $b\ ^3\Pi$-splitting functions with the available experimental data[14,15] insured us that the present relativistic calculations overestimate true SO values by 5–10 % only.

IV. INVERSION PROCEDURE FOR THE $c\ ^3\Sigma^+$, $b\ ^3\Pi$, AND $A\ ^3\Sigma^+$ STATES

Our main goal is to determine the vibrational assignment, molecular constants and accurate RKR potential curve of the $c\ ^3\Sigma^+$ state, to extend the molecular constants and RKR potential for the $b\ ^3\Pi$ state to high vibrational levels $v_b > 49$, as well as to refine the repulsive limb of the $a\ ^3\Sigma^+$ potential near and above the dissociation limit. This will be achieved by multistep inversion procedure based on (1) deperturbation analysis of highly accurate experimental line positions corresponding to the $B\ ^1\Pi \sim c\ ^3\Sigma^+ \sim b\ ^3\Pi \leftarrow X^1\Sigma^+$ transitions measured in Ref. 17, (2) experimental intensity distribution in the bound–bound part of the $c\ ^3\Sigma^+ \rightarrow a\ ^3\Sigma^+$ transition (see Sec. II B), (3) theoretical $B\ ^1\Pi \sim c\ ^3\Sigma^+$ and $c\ ^3\Sigma^+ \sim b\ ^3\Pi$ spin–orbit coupling functions $\xi_{SO}^{el}(R)$, see Sec. III, as well as $c\ ^3\Sigma^+ - a\ ^3\Sigma^+$ and $b\ ^3\Pi - a\ ^3\Sigma^+$ transition dipole moment functions $d(R)$. The highly accurate *ab initio* $c-a$ and $b-a$ dipole moments be-

tween nonrelativistic states of the NaK molecule have been calculated in our previous work[8] using the finite-field (FF) technique combined with the similar MPPT computational scheme, and, hence, they are consistent with the determined SO interaction parameters.

To begin, one needs an initial set of molecular constants for the $c\ ^3\Sigma^+$ and $b\ ^3\Pi$ states which were obtained in the first two steps of the analysis (see below for details) by deperturbation of experimental term values for the $B\ ^1\Pi \sim c\ ^3\Sigma^+ \sim b\ ^3\Pi$ complex.[34] Unambiguous vibrational assignment and the final set of molecular constants for both triplet states were established in the third step from the $c\ ^3\Sigma^+ \rightarrow a\ ^3\Sigma^+$ LIF intensity data, as well as from the absolute values of the vibronic $B\ ^1\Pi \sim c\ ^3\Sigma^+$ and $c\ ^3\Sigma^+ \sim b\ ^3\Pi$ spin–orbit matrix elements. The repulsive limb of the $a\ ^3\Sigma^+$ state was refined by an inversion of the bound–quasibound and bound-free $c\ ^3\Sigma^+ \rightarrow a\ ^3\Sigma^+$ LIF spectra in the last step.

A. Step 1: Deperturbation analysis of the $B\ ^1\Pi \sim c\ ^3\Sigma^+ \sim b\ ^3\Pi$ complex

Rovibronic term values of the perturbed $^{23}Na\,^{39}K\,B\ ^1\Pi \sim c\ ^3\Sigma^+ \sim b\ ^3\Pi$ complex were obtained from highly accurate experimental line positions of the $B\ ^1\Pi \leftarrow X^1\Sigma^+$, $c\ ^3\Sigma^+ \leftarrow X^1\Sigma^+$ and $b\ ^3\Pi \leftarrow X^1\Sigma^+$ transitions measured in Ref. 34 and the refined molecular constants of the ground $X^1\Sigma^+$ state.[26] Most observed bands were assigned in Ref. 34 to mutually perturbed pairs of rovibrational levels corresponding to the $B\ ^1\Pi$ and $c\ ^3\Sigma^+$ states, while five band series were attributed to the spin-forbidden $b\ ^3\Pi_\Omega \leftarrow X^1\Sigma^+$ transitions into different $b\ ^3\Pi$ state Ω-components on the basis of the qualitative picture of their hyperfine structure.[17] However, comprehensive deperturbation analysis of the $b\ ^3\Pi_\Omega \leftarrow X\ ^1\Sigma^+$ bands was not performed to confirm this assignment. At the same time, theoretical structure calculations[2,4] show that the $c\ ^3\Sigma^+$ and $b\ ^3\Pi$ states cross each other in the attractive part of their potential curves near the energy region of the studied $c\ ^3\Sigma^+$ vibrational levels (Fig. 1), and the present relativistic calculations predict a pronounced direct spin–orbit interaction between these states (see Fig. 3). Hence, direct local $c\ ^3\Sigma^+ \sim b\ ^3\Pi$ perturbations seem to be important in this region. This allowed us to reassign the observed $b\ ^3\Pi_\Omega \leftarrow X^1\Sigma^+$ bands to mutually perturbed pairs of vibrational levels belonging to the $b\ ^3\Pi_{\Omega=1}$ and $c\ ^3\Sigma^+$ states coupled with nearest $B\ ^1\Pi$ levels through the $B\ ^1\Pi \sim c\ ^3\Sigma^+$ spin–orbit interaction [see Figs. 4(a), 4(b), and 4(c)]. We have also taken into account that (1) in spite of a large value of the electronic spin–orbit matrix element (Fig. 3), the direct $B\ ^1\Pi \sim b\ ^3\Pi$ interaction is negligible in this energy region due to very small overlap integrals $\langle v_{B\ ^1\Pi} | v_{b\ ^3\Pi} \rangle$ (see Fig. 1), (2) both experimental and theoretical spin–orbit splitting constants of the $b\ ^3\Pi$ state, $A_v^b \approx 15$–$16\ \mathrm{cm}^{-1}$,[7,14] are too large if compared with the observed splitting between the $b\ ^3\Pi_\Omega \leftarrow X^1\Sigma^+$ bands assigned in Ref. 17 to different Ω components of the $b\ ^3\Pi$ state.

The reassigned experimental rovibronic terms of the $B\ ^1\Pi \sim c\ ^3\Sigma^+ \sim b\ ^3\Pi$ complex were approximated by the following effective Hamiltonian matrix:

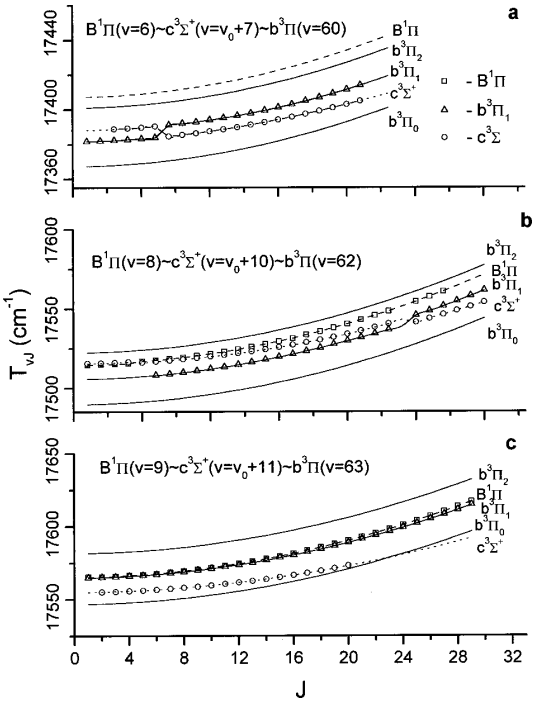

FIG. 4. Experimental (symbols) and calculated (lines) term value positions of the perturbed $B\ ^1\Pi \sim c\ ^3\Sigma^+ \sim b\ ^3\Pi$ complex.

$$
\begin{aligned}
&\langle {}^1\Pi|\mathbf{H}|{}^1\Pi\rangle = T_v^B + B_v^B(X-1) - D_v^B(X-1)^2,\\
&\langle {}^3\Sigma^+|\mathbf{H}|{}^3\Sigma^+\rangle = T_v^c + B_v^c X - D_v^c X^2,\\
&\langle {}^3\Pi_1|\mathbf{H}|{}^3\Pi_1\rangle = T_v^b + B_v^b(X+1) - D_v^b(X^2+6X-3),\\
&\langle {}^3\Pi_0|\mathbf{H}|{}^3\Pi_0\rangle = T_v^b - A_v^b + B_v^b(X+1) - D_v^b(X^2+4X+1),\\
&\langle {}^3\Pi_2|\mathbf{H}|{}^3\Pi_2\rangle = T_v^b + A_v^b + B_v^b(X-3) - D_v^b(X^2-4X+5),\\
&\langle {}^3\Pi_0|\mathbf{H}|{}^3\Pi_1\rangle = -[B_v^b - D_v^b(X+1)]\sqrt{2X},\\
&\langle {}^3\Pi_1|\mathbf{H}|{}^3\Pi_2\rangle = -[B_v^b - 2D_v^b(X-1)]\sqrt{2X-4},\\
&\langle {}^3\Pi_0|\mathbf{H}|{}^3\Pi_2\rangle = -2D_v^b\sqrt{X(X-2)},\\
&\langle {}^1\Pi|\mathbf{H}|{}^3\Sigma^+\rangle = \xi_{v_B v_c}^{B-c},\\
&\langle {}^3\Sigma^+|\mathbf{H}|{}^3\Pi_1\rangle = \xi_{v_c v_b}^{c-b},\\
&\langle {}^3\Sigma^+|\mathbf{H}|{}^3\Pi_0\rangle = -L_{v_c v_b}^{c-b}\sqrt{X},\\
&\langle {}^3\Sigma^+|\mathbf{H}|{}^3\Pi_2\rangle = -L_{v_c v_b}^{c-b}\sqrt{X-2},
\end{aligned}
\tag{1}
$$

where $X = J(J+1)$, $\xi_{v_B v_c}^{B-c}$, and $\xi_{v_c v_b}^{c-b}$ are the nondiagonal rovibronic matrix elements of the spin–orbit interaction between the $B\ ^1\Pi \sim c\ ^3\Sigma^+$ and the $c\ ^3\Sigma^+ \sim b\ ^3\Pi$ state pairs, respectively, and $L_{v_c v_b}^{c-b}$ is the L-uncoupling matrix element between the $c\ ^3\Sigma^+$ and $b\ ^3\Pi$ triplet states. The deperturbed vibronic term values T_v, rotational constants B_v and D_v of both triplet states together with the corresponding spin-orbit matrix elements $\xi_{v_B v_c}^{B-c}$ and $\xi_{v_c v_b}^{c-b}$ were determined by nonlin-

TABLE I. Deperturbed T_v, B_v, and D_v constants for the $c\ ^3\Sigma^+$ and $b\ ^3\Pi$ states of the ^{23}Na ^{39}K molecule (in cm^{-1})

v_c	T_v^c	$B_v^c(10^{-2})$	$D_v^c(10^{-7})$
v_0+1	17 095.87	5.007	3.08
v_0+5	17 293.90	4.672	2.54
v_0+7	17 385.56	4.523	1.90
v_0+8	17 429.36	4.465	2.66
v_0+10	17 514.86	4.303	2.14
v_0+11	17 555.68	4.234	3.12
v_0+13	17 633.90	4.050	3.00
v_0+15	17 707.10	3.942	2.76
v_0+16	17 742.19	3.850	2.90
v_b	T_v^b	$B_v^b(10^{-2})$	$D_v^b(10^{-7})$
60	17 384.25	6.166	3.89
62	17 506.17	5.932	4.20
63	17 564.19	5.814	4.45

ear least-squares fitting of the experimental term values mentioned above. Preliminary vibrational assignment of the $b\ ^3\Pi$ state has been done on the basis of extrapolation of the molecular constants from Ref. 14 to high vibrational levels. To simplify the Hamiltonian matrix approximating the $B\ ^1\Pi \sim c\ ^3\Sigma^+ \sim b\ ^3\Pi$ complex, only such e parity levels which are almost free from hyperfine structure have been incorporated in the deperturbation procedure. The final deperturbed parameters reproduce the experimental term values of the complex with root mean squared deviation of the order of 0.001 cm^{-1} which is comparable with the accuracy of their experimental determination. The experimental term values assigned to the $B\ ^1\Pi(v=6) \sim c\ ^3\Sigma^+(v=v_0+7) \sim b\ ^3\Pi(v=60)$ and $B\ ^1\Pi(v=8) \sim c\ ^3\Sigma^+(v=v_0+10) \sim b\ ^3\Pi(v=62)$ complex were found to be almost insensitive to the fitting parameters A_v^b and L_{v_c,v_b}^{c-b} because the relevant $b\ ^3\Pi_0$ and $b\ ^3\Pi_2$ components [see Figs. 4(a) and 4(b)] are too far from the region in which the perturbation has been observed. On the contrary, for the $B\ ^1\Pi(v=9) \sim c\ ^3\Sigma^+(v=v_0+11) \sim b\ ^3\Pi(v=63)$ complex, where a pseudocrossing of the observed $c\ ^3\Sigma^+$ state and the ''dark'' $b\ ^3\Pi_0$ component takes place [Fig. 4(c)], the corresponding $A_{v=63}^b = 15.7(1)$ and $L_{v_c=v_0+11,v_b=63}^{c-b} = 0.0046(2)$ values (in cm^{-1}) were determined with acceptable accuracy.

The remaining experimental term values assigned to the pairs of the mutually interacting levels of the $B\ ^1\Pi \sim c\ ^3\Sigma^+$ complex were processed by the simplest two-level deperturbation analysis based on the reduced Hamiltonian matrix (1):

$$\begin{aligned} \langle {}^1\Pi|\mathbf{H}|{}^1\Pi\rangle &= T_v^B + B_v^B(X-1) - D_v^B(X-1)^2, \\ \langle {}^3\Sigma^+|\mathbf{H}|{}^3\Sigma^+\rangle &= T_v^c + B_v^c X - D_v^c X^2, \\ \langle {}^1\Pi|\mathbf{H}|{}^3\Sigma^+\rangle &= \xi_{v_B v_c}^{B-c} \end{aligned} \tag{2}$$

using the fixed set of deperturbed molecular constants for the $B\ ^1\Pi$ state.[20] The resulting $c\ ^3\Sigma^+$ state molecular constants for vibrational levels from v_0+1 to v_0+16, where v_0 is the unknown first vibrational level of $c\ ^3\Sigma^+$ lying above the level $v=0$ of the $B\ ^1\Pi$ state, are presented in Table I. The corresponding experimental $B\ ^1\Pi \sim c\ ^3\Sigma^+$ and $c\ ^3\Sigma^+ \sim b\ ^3\Pi$ spin-orbit matrix elements $\xi_{v_B v_c}^{B-c}$ and $\xi_{v_c v_b}^{c-b}$ are given in Table II.

TABLE II. Experimental and calculated spin–orbit matrix elements $\xi_{v_B v_c}^{B-c}$ and $\xi_{v_c v_b}^{c-b}$ (in cm^{-1}) for $B\ ^1\Pi \sim c\ ^3\Sigma^+$ and $b\ ^3\Pi \sim c\ ^3\Sigma^+$ pairs of the interacting states of the ^{23}Na ^{39}K molecule.

		Experimental		Calculated		
				$\xi_{v_B v_c}^{B-c}$		
$v_B \sim v_c$	J_c	This work	Ref. 18	$v_0=19$	$v_0=20$	$v_0=21$
$4 \sim v_0+5$	13	0.157	0.159	0.28	0.17	0.10
$6 \sim v_0+8$	33	0.239	0.22	0.40	0.25	0.15
$8 \sim v_0+10$	5	0.408	0.400	0.67	0.44	0.28
$8 \sim v_0+11$	46		0.266	0.47	0.30	0.19
$9 \sim v_0+11$	10	0.54		0.77	0.53	0.34
$9 \sim v_0+12$	40		0.34	0.59	0.39	0.24
$10 \sim v_0+13$	33		0.44	0.70	0.47	0.30
$11 \sim v_0+14$	25		0.50	0.80	0.56	0.36
$12 \sim v_0+15$	14	0.578	0.58	0.89	0.64	0.42
Average deviation (%)				**64**	**9**	**32**
$v_b \sim v_c$				$\xi_{v_c v_b}^{c-b}$		
$60 \sim v_0+7$	13	3.243		2.95	3.20	1.98
$62 \sim v_0+10$	24	2.013		0.05	1.94	2.65
$63 \sim v_0+11$	15	2.500		1.03	2.47	2.37
Average deviation (%)				**55**	**2**	**25**

B. Step 2: RKR potentials

1. $c\ ^3\Sigma^+$ state

The deperturbed T_v and B_v constants of the $c\ ^3\Sigma^+$ state from Table I were then approximated by the series

$$\begin{aligned} T_v &= T_e + \omega_e v - \omega_e x_e v^2 + \omega_e y_e v^3, \\ B_v &= B_e - \alpha_e v + \gamma_e v^2, \\ D_v &= D_e + \beta_{e1} v + \beta_{e2} v^2, \end{aligned} \tag{3}$$

where $v = v_0 + n + 1/2$. A usual way to determine the required molecular constants which enter Eq. (3) would be to accomplish a conventional linear least-squares fit of the T_v and B_v values, as it was done in Refs. 17 and 20. Unfortunately, such an inversion procedure leads to large extrapolation errors in equilibrium molecular constants ω_e and B_e since the experimental T_v and B_v values are available only for large v values. To minimize extrapolation error, we fit T_v and B_v using fixed ω_e and B_e parameters taken from *ab initio* calculations since the latter are *a priori* more accurate than the ones obtained from the extrapolation procedure. An additional argument to use *ab initio* equilibrium constants is that essentially different electronic structure calculations produced very close ω_e and B_e values, see Table V of Ref. 4. We adopted the fixed values $\omega_e = 73.4$ cm^{-1} and $B_e = 0.062\,75$ cm^{-1} from Ref. 4 as the most reliable, and obtained the remaining molecular constants (T_e, $\omega_e x_e$, $\omega_e y_e$, α_e, and γ_e) by a linear least-squares fitting for each particular v_0 value from 12 to 25. Then, the adiabatic potential curves corresponding to each set of molecular constants were

TABLE III. The Dunham constants (in cm^{-1}) for the $b\ ^3\Pi$ state of the $^{23}Na\ ^{39}K$ molecule ($T_e = 11\ 562.18\ cm^{-1}$).

Y_{10}	120.371 380	Y_{01}	$0.950\ 673\times10^{-1}$	Y_{02}	$-0.230\ 157\times10^{-6}$
Y_{20}	−0.332 024	Y_{11}	$-0.328\ 708\times10^{-3}$	Y_{12}	$-0.178\ 322\times10^{-8}$
Y_{30}	$-0.104\ 098\times10^{-2}$	Y_{21}	$-0.205\ 156\times10^{-5}$	Y_{22}	$0.802\ 326\times10^{-10}$
Y_{40}	$0.386\ 127\times10^{-4}$	Y_{31}	$0.361\ 430\times10^{-7}$	Y_{32}	$-0.159\ 840\times10^{-11}$
Y_{50}	$-0.123\ 100\times10^{-5}$	Y_{41}	$-0.186\ 723\times10^{-8}$		
Y_{60}	$0.143\ 700\times10^{-7}$	Y_{51}	$0.278\ 352\times10^{-10}$		
Y_{70}	$-0.805\ 024\times10^{-10}$	Y_{61}	$-0.235\ 550\times10^{-12}$		

constructed by the RKR procedure. Experimental D_v values from Table I were fitted with a fixed value of D_e estimated from the relation $D_e = 4B_e^3/\omega_e^2$.[24]

2. $b\ ^3\Pi$ state

The deperturbed T_v, B_v and D_v values derived for the $v_b = 60$,62, and 63 vibrational levels of the $b\ ^3\Pi$ state (Table I) were simultaneously fitted by the Dunham series with the corresponding data for the lowest $v_b = 0-49$ levels taken from Ref. 9. The resulting molecular constants which are now valid up to $v_b = 63$ are presented in Table III.

C. Step 3: determination of v_0 for the $c\ ^3\Sigma^+$ state

1. LIF intensity distribution

Rovibrational eigenvalues E_v^N and eigenfunctions $|v_c(N)\rangle$ corresponding to each of the 14 derived RKR potentials of the $c\ ^3\Sigma^+$ state obtained in the previous step were calculated numerically by solving the radial Schrödinger equation.[27] The relevant intensities of rovibronic $c\ ^3\Sigma^+ \rightarrow a\ ^3\Sigma^+$ transitions for the bound–bound part of the spectrum were then evaluated as:

$$I_{v_c' v_a''}^{N'N''} \sim \nu^4 |\langle v_c'(N')|d_{c-a}|v_a''(N'')\rangle_R|^2 S_{^3\Sigma^+ - ^3\Sigma^+}^{N'N''}, \qquad (4)$$

where $\nu = E_{v_c'}^{N'} - E_{v_a''}^{N''}$ is the rovibronic transition wave number, $S_{^3\Sigma^+ - ^3\Sigma^+}^{N'N''}$ are the Hönl–London factors of a $^3\Sigma^+ - ^3\Sigma^+$ transition[35] and $d_{c-a}(R)$ is the $c\ ^3\Sigma^+ - a\ ^3\Sigma^+$ transition dipole moment taken from Ref. 8. The bound vibrational energy $E_{v_a''}^{N''}$ and eigenfunctions $|v_a''(N'')\rangle$ of the $a\ ^3\Sigma^+$ state have been calculated using the IPA potential from Ref. 10. By comparing the calculated $I_{v_c' v_a''}^{N'N''}$ values with the respective experimental relative intensity distribution in the bound–bound part of the $c\ ^3\Sigma^+ \rightarrow a\ ^3\Sigma^+$ spectra measured in the present work (see Sec. II B), we determined unambiguously that the theoretical probabilities $I_{v_c' v_a''}^{N'N''}$ agree with the experimental ones only for $v_0 = 20$ (see Figs. 5–7). Figure 5 demonstrates the sensitivity of this routine with respect to v_0: it can be clearly seen that even the neighboring values $v_0 = 19$ and 21 do not produce satisfactory agreement with the experimental intensity pattern. Besides, we were able to reproduce the $c\ ^3\Sigma^+ \rightarrow a\ ^3\Sigma^+$ bound–bound part intensity distribution given in Fig. 8 of Ref. 20 when the $a\ ^3\Sigma^+$ state vibrational numbers were increased by one to match the correct vibrational assignment.

Since bound–free parts of the experimental $c\ ^3\Sigma^+ \rightarrow a\ ^3\Sigma^+$ progressions (Sec. II) are also available, we simulated these patterns using the relation

$$I_{v_c'}^{N'}(\nu) \sim \sum_{N''} \nu^4 |\langle v_c'(N')|d_{c-a}|E_a(N'')\rangle_R|^2 S_{^3\Sigma^+ - ^3\Sigma^+}^{N'N''}, \qquad (5)$$

where the bound eigenfunctions $|v_c(N)\rangle$ correspond to different assignments $v_0 = 19$, 20, and 21, whereas the unbound eigenfunctions $|E_a(N'')\rangle$ were calculated with the empirical $a\ ^3\Sigma^+$ potential from Ref. 11. As already shown in Ref. 12, a direct comparison of the calculated $I_{v_c'}^{N'}(\nu)$ values with their experimental counterparts unambiguously confirmed the $v_0 = 20$ assignment as well.

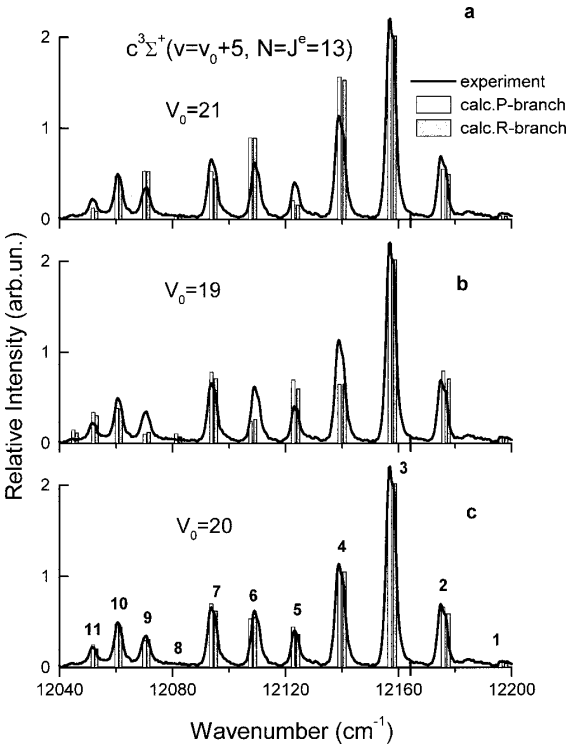

FIG. 5. Comparison of the experimental bound–bound $c\ ^3\Sigma^+ \rightarrow a\ ^3\Sigma^+$ emission from a single level in the $c\ ^3\Sigma^+$ state with the spectrum simulated using different v_0 assignments. Numbers on the top of the peaks denote vibrational assignment of the $a\ ^3\Sigma^+$ state.

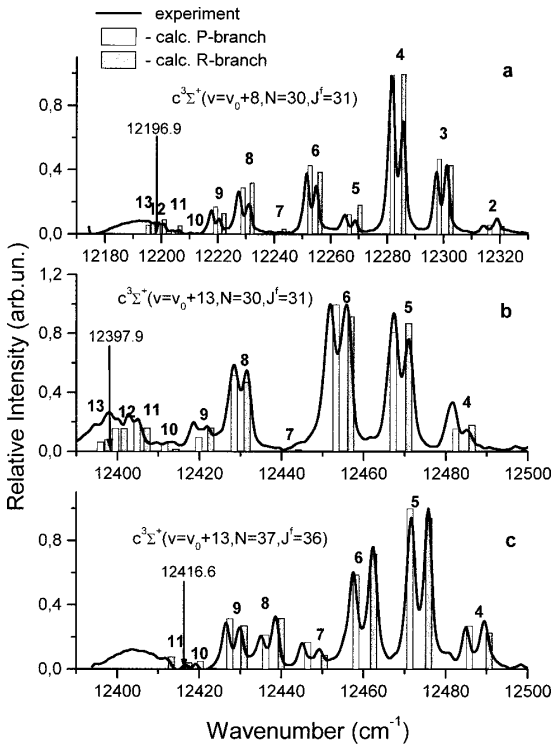

FIG. 6. Experimental $c\ ^3\Sigma^+ \rightarrow a\ ^3\Sigma^+$ LIF spectra and simulated ones with $v_0=20$. The arrows show the border of bound–bound and bound–quasibound parts of spectra. Numbers denote vibrational assignment of the $a\ ^3\Sigma^+$ state.

2. SO coupling constants

In order to get independent justification of the present vibrational assignment and to check the accuracy of the derived RKR potentials for the $c\ ^3\Sigma^+$ and $b\ ^3\Pi$ states, it makes sense to invoke the experimental values of rovibronic spin-orbit matrix elements of the $B\ ^1\Pi \sim c\ ^3\Sigma^+$ and $c\ ^3\Sigma^+ \sim b\ ^3\Pi$ coupling (Table II) since it is clear that these values are sensitive enough to the shape of the potential curve.[24] In doing so, the vibrational eigenfunctions of the $c\ ^3\Sigma^+$ state corresponding to the $v_0=19$,20, and 21 assignments were used in the calculation of the respective matrix elements:

$$\xi^{B-c}_{v_B v_c}=|\langle v^J_B|\xi^{B-c}_{\mathrm{SO}}|v^J_c\rangle_R|, \quad \xi^{c-b}_{v_c v_b}=|\langle v^J_b|\xi^{c-b}_{\mathrm{SO}}|v^J_c\rangle_R|, \quad (6)$$

where $\xi^{B-c}_{\mathrm{so}}(R)$ and $\xi^{c-b}_{\mathrm{so}}(R)$ are the electronic spin–orbit matrix elements calculated in Sec. III. Here $|v^J_b\rangle$ are vibrational eigenfunctions of the $b\ ^3\Pi$ state computed with the RKR potential based on the molecular constants from Table III, while $|v^J_B\rangle$ are the vibrational eigenfunctions of the $B\ ^1\Pi$ state obtained with the RKR potential from Ref. 20. Table II unambiguously shows that the calculated $\xi^{B-c}_{v_B v_c}$ and $\xi^{c-b}_{v_c v_b}$ values reach maximal quantitative agreement with the respective experimental data at $v_0=20$ only.

It should be noted that the overlap integral between the triplet states $\langle v_c=v_0+n|v_b\rangle$ is an oscillating function of the v_0 value, while its singlet–triplet counterpart $\langle v_B|v_c=v_0+n\rangle$ is a monotonic one. Hence, the $\langle v_b|v_c\rangle$ values are generally more sensitive to the vibrational numbering of the $c\ ^3\Sigma^+$ state than the $\langle v_B|v_c\rangle$ ones. It should also be noted that the overlap integrals between all states studied here are very sensitive to rotational quantum numbers of the involved radiative and nonradiative transitions since the respective potential curves are shifted from each other significantly[36] (see Fig. 1). Thus, vibrational eigenfunctions of all the above-mentioned states were calculated with RKR or IPA rotationless potentials plus the centrifugal distortion term which takes properly into account the rotational effect in explicit form.[37]

The resulting molecular constants of the $c\ ^3\Sigma^+$ state corresponding to the $v_0=20$ assignment, as well as the relevant RKR potential are given in Tables IV and V, respectively. The self-consistency of the $c\ ^3\Sigma^+$ constants has been additionally proved by the following facts: (1) the Dunham correction $Y_{00}=0.0063\ \mathrm{cm}^{-1}$ is small enough; (2) the fitted α_e parameter (see Table II) agrees well with its value calculated from the Pekeris relation:[38] $\alpha_e^{\mathrm{Pekeris}}=5.685\times10^{-4}\ \mathrm{cm}^{-1}$; (3) the calculated dissociation energy (in cm^{-1})

$$D^{c\ ^3\Sigma^+}_{\mathrm{dis}}=D^{X\ ^1\Sigma^+}_{\mathrm{dis}}+\Delta E[K(4p^2P_{1/2})-K(4s^2S_{1/2})]-T^{c\ ^3\Sigma^+}_e = 2508 \quad (7)$$

is in very good agreement with the respective perturbed-Morse-oscillator (PMO) model estimate[39]: $D^{\mathrm{PMO}}_{\mathrm{dis}}=2564$.

Finally, the theoretical A^b_v and $L^{c-b}_{v_c v_b}$ values for all studied triplet vibronic terms were estimated using the following relations:

$$A^b_v=|\langle v_b|\xi^{b\ ^3\Pi}_{\mathrm{SO}}|v_b\rangle_R|, \quad L^{c-b}_{v_c v_b}=L^{c-b}_{\mathrm{el}}\left|\langle v_b|\frac{1}{2mR^2}|v_c\rangle_R\right|, \quad (8)$$

where $|v_b\rangle$ and $|v_c\rangle$ are vibrational eigenfunctions corresponding to the derived RKR potentials for the interacting $c\ ^3\Sigma^+$ and $b\ ^3\Pi$ states, m is the molecular reduced mass and $L^{c-b}_{\mathrm{el}}=\langle b\ ^3\Pi|\mathbf{L}|c\ ^3\Sigma^+\rangle$ is the electronic L-uncoupling matrix element between the triplet states. The empirical L^{c-b}_{el}

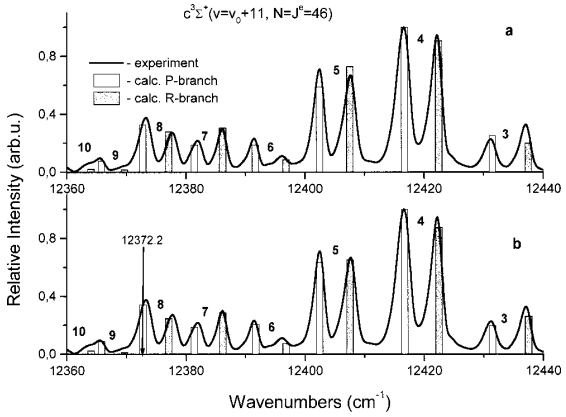

FIG. 7. A comparison of the experimental bound–bound emission with the calculated spectrum obtained (a) in adiabatic approximation by Eq. (4) and (b) in nonadiabatic approximation by Eq. (9).

TABLE IV. The molecular constants (in cm^{-1}) for the $c\ ^3\Sigma^+$ state of the $^{23}Na\ ^{39}K$ molecule obtained by different methods.

	This work ($v_0=20$)	Ref. 17 ($v_0=16$)	Ref. 20 ($v_0=12$)	Ref. 12 ($v_0=20$)
T_e	15 750.64	15 988.485	16 283.595	15 857
ω_e	73.4[a]	73.7944	68.6431	63.17
$\omega_e x_e$	0.480 173	0.649 417	0.638 45	0.1615
$\omega_e y_e$	$-9.824\ 85\times10^{-4}$	$9.142\ 19\times10^{-4}$	$9.143\ 29\times10^{-4}$	-4.18×10^{-3}
B_e	0.062 75[a]	0.069 281 5	0.064 307 6	0.0588
α_e	$5.914\ 25\times10^{-4}$	$1.285\ 40\times10^{-3}$	$1.201\ 57\times10^{-3}$	3.0×10^{-4}
γ_e	$-1.810\ 58\times10^{-6}$	$1.047\ 89\times10^{-5}$	$1.047\ 89\times10^{-5}$	-7.4×10^{-6}
D_e	1.83×10^{-7}[b]	2.443×10^{-7}	2.443×10^{-7}	
β_{e1}	3.45×10^{-9}			
β_{e2}	-2.17×10^{-11}			

[a]Fixed *ab initio* value taken from Ref. 4.
[b]Estimated by the relation $D_e=4B_e^3/\omega_e^2$.

matrix element was determined by a comparison of the calculated $|\langle v_b=63|1/2mR^2|v_c=33\rangle_R|$ integral with the experimental $L^{c-b}_{v_c=33,v_b=63}$value obtained in Sec. IV A. It is interesting that the obtained $L^{c-b}_{\rm el}=0.82$ value for the triplet–triplet interaction appeared to be very close to the empirical value $L^{B-C}_{\rm el}=\langle B\ ^1\Pi|\mathbf{L}|C^1\Sigma^+\rangle=0.75$ derived for its singlet–singlet counterpart.[5] The calculated $A^b_{v=63}=16.5\ cm^{-1}$ value is also in very good agreement with the experimental value obtained in Sec. IV A.

Thus, it seems that all these tests are demonstrating reliability of the present molecular parameters.

D. Step 4: Updated $a\ ^3\Sigma^+$ potential near and above the dissociation limit

As a result of the previous steps, we now possess the following data: (i) the uniquely determined RKR potential of the $c\ ^3\Sigma^+$ state (Sec. IV); (ii) the full experimental $c\ ^3\Sigma^+ \rightarrow a\ ^3\Sigma^+$ transition patterns for four progressions (Sec II); (iii) the accurate theoretical $c\ ^3\Sigma^+ - a\ ^3\Sigma^+$ transition dipole moment.[8] It seems quite reasonable to use all of this data in order to refine the $a\ ^3\Sigma^+$ state repulsive limb near and above the dissociation limit which should be a smooth continuation of the $a\ ^3\Sigma^+$ state IPA potential given for the bound region in Ref. 10. To realize this approach, we have performed a full quantum-mechanical trial-and-error inversion of the experimental bound–quasibound and bound–free spectra mentioned above using the relations given by Eqs. (4) and (5). As a first approximation we used the empirical repulsive potential from Ref. 11 as the most accurate one. Since this potential reproduces, with satisfactory accuracy, the bound–free $c\ ^3\Sigma^+ - a\ ^3\Sigma^+$ spectra (see step 3), two iterations appeared to be sufficient to obtain the final potential reproducing all five experimental spectra (Sec.II) within their experimental accuracy limit; see Fig. 8 as an example. The derived potential (see Fig. 9) which is valid for $3.3\ Å < R < 4.6\ Å$, matches smoothly the IPA potential[10] at the point $R=4.62$ Å. This allows one to describe continuously all bound, quasibound, and unbound $a\ ^3\Sigma^+$ state levels.

V. RADIATIVE PROPERTIES OF THE $B\ ^1\Pi \sim c\ ^3\Sigma^+ \sim b\ ^3\Pi$ COMPLEX

The $B\ ^1\Pi \sim c\ ^3\Sigma^+ \sim b\ ^3\Pi$ interaction analyzed in Sec. IV A should apparently manifest itself in the radiative properties of the complex as well. The $B\ ^1\Pi \sim c\ ^3\Sigma^+$ interaction does not affect the relative intensities of the $c\ ^3\Sigma^+ \rightarrow a\ ^3\Sigma^+$ spectra since singlet-triplet transitions are strongly forbidden in the adiabatic approximation, whereas the

TABLE V. The rotationless RKR potential corresponding to the $v_0=20$ assignment of the $c\ ^3\Sigma^+$ state of the $^{23}Na\ ^{39}K$ molecule. Note that *ab initio* values (Ref. 4) of ω_e and B_e are assumed. The corresponding *ab initio* value of $R_e=4.3075$ Å.

v	E_v (cm^{-1})	$R_{\rm min}$ (Å)	$R_{\rm max}$ (Å)
0	36.59	4.1422	4.4997
1	109.02	4.0309	4.6535
2	180.49	3.9596	4.7679
3	250.98	3.9047	4.8666
4	320.49	3.8593	4.9564
5	389.02	3.8204	5.0405
6	456.55	3.7862	5.1206
7	523.08	3.7556	5.1978
8	588.61	3.7279	5.2729
9	653.13	3.7025	5.3464
10	716.63	3.6792	5.4188
11	779.11	3.6576	5.4903
12	840.56	3.6375	5.5611
13	900.98	3.6187	5.6317
14	960.35	3.6011	5.7020
15	1018.69	3.5844	5.7723
16	1075.97	3.5687	5.8427
17	1132.19	3.5538	5.9133
18	1187.35	3.5397	5.9843
19	1241.44	3.5263	6.0558
20	1294.45	3.5135	6.1278
21	1346.38	3.5012	6.2006
22	1397.23	3.4895	6.2741
23	1446.98	3.4783	6.3485
24	1495.63	3.4675	6.4240
25	1543.18	3.4571	6.5006
26	1589.62	3.4471	6.5783
27	1634.94	3.4374	6.6574
28	1679.14	3.4280	6.7380
29	1722.21	3.4188	6.8201
30	1764.15	3.4100	6.9040
31	1804.95	3.4013	6.9897
32	1844.60	3.3928	7.0773
33	1883.09	3.3845	7.1672
34	1920.44	3.3763	7.2593
35	1956.61	3.3683	7.3540
36	1991.62	3.3602	7.4514

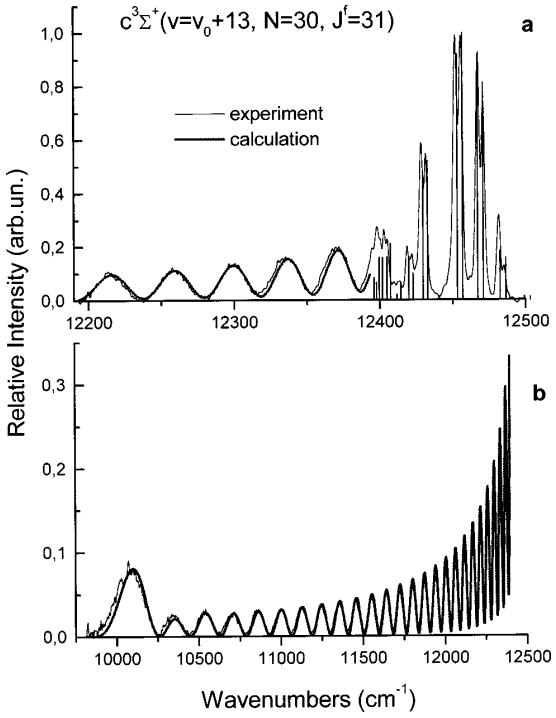

FIG. 8. The full experimental LIF emission pattern, obtained in present work (a) and in Ref. 12 (b) and their theoretical counterparts calculated with the present $c\ ^3\Sigma^+$ and $a\ ^3\Sigma^+$ potentials.

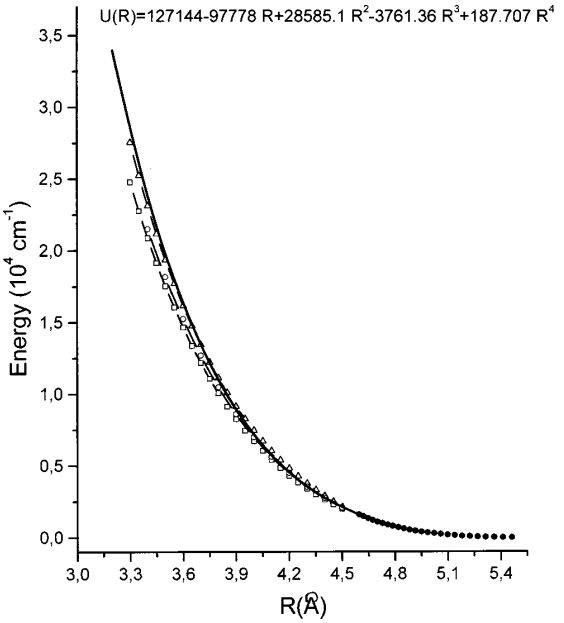

FIG. 9. Comparison of the experimental $a\ ^3\Sigma^+$ repulsive walls obtained in the present work (bold solid line) with those determined by an inversion of the $b\ ^3\Pi \rightarrow a\ ^3\Sigma^+$ (Ref. 11, open triangles), $d^3\Pi \rightarrow a\ ^3\Sigma^+$ (Ref. 13, open squares) and $c\ ^3\Sigma^+ \rightarrow a\ ^3\Sigma^+$ (Ref. 12, open circles) bound-free spectra. The full circles for $R>4.6$(Å) denote the bound portion of the IPA potential from Ref. 10. The analytical formula for the proposed potential curve is given above.

$c\ ^3\Sigma^+ \sim b\ ^3\Pi$ perturbation should lead to intensity redistribution in the rotational structure of the $c\ ^3\Sigma^+ \rightarrow a\ ^3\Sigma^+$ spectra due to the interference effect between the adiabatic $c \rightarrow a$ and $b \rightarrow a$ transitions:

$$I^{J'N'N''}_{v'_c v'_b v''_a} \sim \nu^4 \left[C_{^3\Sigma^+} \langle v'_c(N') | d_{c-a} | v''_a(N'') \rangle_R F^{N'N''}_{^3\Sigma^+ - ^3\Sigma^+} + \sum_{\Omega=0}^{2} C_{^3\Pi_\Omega} \langle v'_b(J') | d_{b-a} | v''_a(N'') \rangle_R F^{J'N''}_{^3\Pi_\Omega - ^3\Sigma^+} \right]^2, \tag{9}$$

where $d_{b-a}(R)$ is the $b\ ^3\Pi - a\ ^3\Sigma^+$ transition dipole moment from Ref. 8, $C_{^3\Sigma^+}$and $C_{^3\Pi_\Omega}$are mixing coefficients for the $c\ ^3\Sigma^+$ and $b\ ^3\Pi_\Omega$ interacting states, and $F^{N'N''}_{^3\Sigma^+ - ^3\Sigma^+}$and $F^{J'N''}_{^3\Pi_\Omega - ^3\Sigma^+}$ are the overlap integrals between the respective rotational eigenfunctions.[35]

In contrast to the adiabatic approximation, nonadiabatic radiative lifetimes of the complex ($\tau^{N'}_{\text{pert}}$) constitute a sum of all adiabatic transition probabilities into both lower-lying singlet ($X^1\Sigma^+$) and triplet ($a\ ^3\Sigma^+$) states:

$$(\tau^{N'}_{\text{pert}})^{-1} \approx C^2_{^1\Pi} / \tau^{\text{ad}}_{v'_B} + C^2_{^3\Sigma} / \tau^{\text{ad}}_{v'_c} + C^2_{^3\Pi} / \tau^{\text{ad}}_{v'_b},$$

where $C_{^1\Pi}$ is the mixing coefficient of the $B\ ^1\Pi$ state, whereas $\tau^{\text{ad}}_{v'_B}$, $\tau^{\text{ad}}_{v'_b}$, and $\tau^{\text{ad}}_{v'_c}$ are the adiabatic lifetimes of the $B\ ^1\Pi$, $b\ ^3\Pi$, and $c\ ^3\Sigma^+$ states, respectively. To avoid tedious integration over the energy corresponding to the long unbound parts of the $c\ ^3\Sigma^+ \rightarrow a\ ^3\Sigma^+$ and $b\ ^3\Pi \rightarrow a\ ^3\Sigma^+$ spectra, the adiabatic lifetimes of the triplet states have been approximated by the relations[40]

$$1/\tau^{\text{ad}}_{v'_c} \approx K \langle v'_c | [U_c - U_a]^3 d^2_{c-a} | v'_c \rangle_R,$$
$$1/\tau^{\text{ad}}_{v'_b} \approx K \langle v'_b | [U_b - U_a]^3 d^2_{b-a} | v'_b \rangle_R, \tag{10}$$

where $K = 64\pi^4/3h^2$, whereas $U_a(R)$, $U_b(R)$ and $U_c(R)$ are the adiabatic potential curves obtained in the preceding section for the $a\ ^3\Sigma^+$, $b\ ^3\Pi$, and $c\ ^3\Sigma^+$ states. The relevant adiabatic $\tau^{\text{ad}}_{v'_B}$ values were obtained in Ref. 6 under the same approximation.

In order to analyze available experimental data by the relations (9) and (10), the required mixing coefficients for the respective adiabatic states have been estimated by diagonalization of the Hamiltonian matrix (1) involving the deperturbed molecular parameters obtained in Sec. IV. These calculations demonstrate that rovibronic levels of the $B\ ^1\Pi \sim c\ ^3\Sigma^+ \sim b\ ^3\Pi$ complex treated in Sec. IV A are subject to strong local $B\ ^1\Pi \sim c\ ^3\Sigma^+$ and $b\ ^3\Pi \sim c\ ^3\Sigma^+$ perturbations while the five $c\ ^3\Sigma^+$ levels investigated in Sec. II undergo strong local $B\ ^1\Pi \sim c\ ^3\Sigma^+$ and weak regular $b\ ^3\Pi \sim c\ ^3\Sigma^+$ perturbations, with the pronounced $b\ ^3\Pi \sim c\ ^3\Sigma^+$ interaction for the $v_c = v_0 + 11$, $N = J^e = 46$ level only.

The computed nonadiabatic τ values for the strongly perturbed rovibronic levels considered in Sec. IV A are presented in Fig. 10. Lifetime measurements performed in Ref.

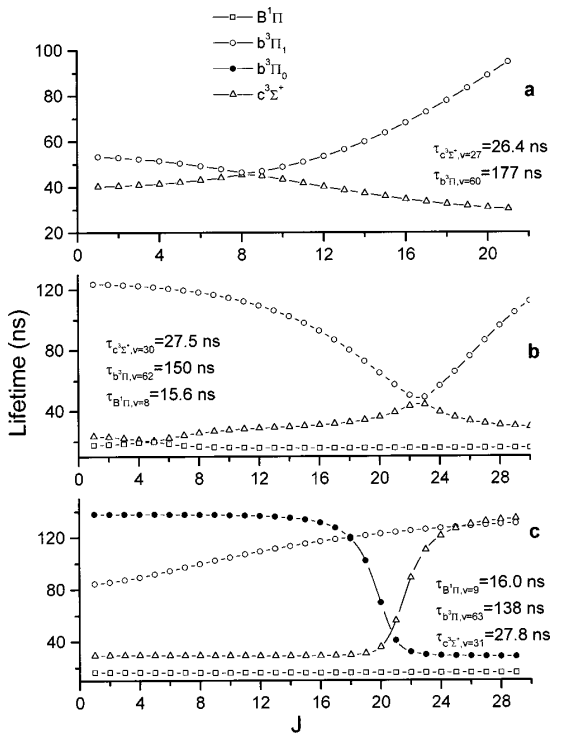

FIG. 10. Calculated nonadiabatic lifetimes for strongly perturbed levels of the $B\ ^1\Pi \sim c\ ^3\Sigma^+ \sim b\ ^3\Pi$ complex. The τ values for a particular state given in the figure denote the adiabatic lifetimes for the corresponding vibrational levels.

41 indicate that the radiative τ values of the perturbed levels at about 17 500 cm^{-1} should range between 20–25 ns. As can be seen from Fig. 10(b), the present estimates confirm these data. The simulated bound–bound $c\ ^3\Sigma^+ \rightarrow a\ ^3\Sigma^+$ LIF spectrum originating from the weakly perturbed $v_c = v_0 + 11$, $N = J^e = 46$ level mentioned above is presented in Fig. 7(b). A comparison of the spectrum evaluated by Eq. (4) in adiabatic approximation [Fig. 7(a)] with the one calculated by Eq. (9) in nonadiabatic approximation [Fig. 7(b)] shows that the inclusion of $b\ ^3\Pi \sim c\ ^3\Sigma^+$ interaction slightly improves the agreement between the theoretical and experimental intensity distributions of the rotational structure. It can also be seen that such improvement is pronounced only for the rotational doublets corresponding to the lowest vibrational $a\ ^3\Sigma^+$ levels since the magnitude of the $b-a$ transition dipole moment becomes comparable with the $c-a$ transition dipole moment only at large internuclear distances.[3,8]

VI. CONCLUDING REMARKS

(1) The controversy in vibrational numbering of the $c\ ^3\Sigma^+$ state deduced from the bound–bound and bound-free LIF intensities disappears after revising the $a\ ^3\Sigma^+$ state vibrational assignment in bound–bound LIF progressions (see Figs. 5–7).

(2) Vibrational assignment by the perturbation matrix element method,[24] based on the independence of the $\langle v_i|\xi_{SO}^{el}(R)|v_j\rangle/\langle v_i|v_j\rangle$ ratios on vibrational levels, fails in the case of the $B\ ^1\Pi \sim c\ ^3\Sigma^+$ SO coupling because of monotonic dependence of overlap integrals on v_0 numbering. Such dependence is caused by the fact that the levels under study are below the crossing point of the repulsive walls of the $B\ ^1\Pi$ and $c\ ^3\Sigma^+$ states, see Fig. 1. However, the overlap integrals are exponentially small and their absolute values are very sensitive to the value of v_0. Therefore if the electronic part of the SO matrix element is available from the highly accurate relativistic calculations, the vibrational numbering may be established unambiguously by direct comparison of calculated $|\langle v_i|\xi_{SO}^{el}(R)|v_j\rangle|$ and experimental $\xi_{SO}^{v_i v_j}$ values, see Table II.

(3) Contrary to the $B\ ^1\Pi \sim c\ ^3\Sigma^+$ interaction, in the case of $b\ ^3\Pi \sim c\ ^3\Sigma^+$ coupling the perturbation matrix element method[24] works properly due to the oscillatory behavior of the overlap integrals, since the levels under study are situated near and above the crossing point of the attractive walls of the interacting states (see Fig. 1).

(4) The simultaneous treatment of the $B\ ^1\Pi$, $c\ ^3\Sigma^+$, and $b\ ^3\Pi$ mutually perturbed states made it possible to reassign the Ω components of the $b\ ^3\Pi_\Omega$ state. As a result, the molecular constants of the $b\ ^3\Pi$ state have been extended up to $v_b = 63$ (see Table III).

(5) The derived accurate adiabatic $c\ ^3\Sigma^+$ potential along with the calculated $c\ ^3\Sigma^+ - a\ ^3\Sigma^+$ transition dipole moment and full bound–bound, bound–quasibound, and bound-free intensity patterns allow us to refine the $a\ ^3\Sigma^+$ potential (see Fig. 9).

(6) The influence of the $b\ ^3\Pi \sim c\ ^3\Sigma^+$ perturbation on the intensity distribution of the $c\ ^3\Sigma^+ \rightarrow a\ ^3\Sigma^+$ transition and the radiative lifetimes of the $B\ ^1\Pi \sim c\ ^3\Sigma^+ \sim b\ ^3\Pi$ complex have been investigated for the cases of strong local and weak regular interactions.

ACKNOWLEDGMENTS

The experimental part of this work has become possible due to the financial support from the USA National Research Council Twinning Program 1997–1999 with Estonia, Latvia and Lithuania. Financial support by the Russian Foundation of Basic Researches under Grants No. 97-03-32215 and No. 97-03-33714 is gratefully acknowledged by the Moscow group. R.F. is grateful to the Latvian Science Council (Grant No. 96.0323), P.K. to the Polish Committee for Scientific Research (Grant No. 2 PO3B 067 16), and W.C.S. to the U.S. National Science Foundation (Grant No. CHE 9732467). The authors would like to thank Dr. Sylvie Magnier, Professor Hajime Katô, and Professor Warren Zemke for placing unpublished information at our disposal, as well as Dr. Maris Tamanis for useful discussions.

[1] G.-H. Jeung, J.-P. Daudey, and J.-P. Malrieu, Chem. Phys. Lett. **94**, 300 (1983).
[2] W. J. Stevens, D. D. Konowalow, and L. B. Ratcliff, J. Chem. Phys. **80**, 1215 (1984).
[3] L. B. Ratcliff, D. D. Konowalow, and W. J. Stevens, J. Mol. Spectrosc. **110**, 242 (1985).
[4] S. Magnier and Ph. Millé, Phys. Rev. A **54**, 204 (1996).
[5] M. Tamanis, M. Auzinsh, I. Klincare, O. Nikolayeva, R. Ferber, E. A. Pazyuk, A. V. Stolyarov, and A. Zaitsevskii, Phys. Rev. A **58**, 1932 (1998).

[6] M. Tamanis, M. Auzinsh, I. Klincare, O. Nikolayeva, R. Ferber, A. Zaitsevskii, E. A. Pazyuk and A. V. Stolyarov, J. Chem. Phys. **109**, 6725 (1998).
[7] E. A. Pazyuk, A. V. Stolyarov, A. Zaitsevskii, R. Ferber, P. Kowalczyk, and Ch. Teichteil, Mol. Phys. **96**, 955 (1999).
[8] E. A. Pazyuk, A. V. Stolyarov, and A. Zaitsevskii, Opt. Spectrosc. **87**, 225 (1999).
[9] A. J. Ross, C. Effantin, J. d'Incan, and R. F. Barrow, Mol. Phys. **56**, 903 (1985).
[10] K. Ishikawa, N. Mukai, and M. Tanimura, J. Chem. Phys. **101**, 876 (1994).
[11] M. Masters, J. Huennekens, W.-T. Luh, L. Li, A. M. Lyyra, K. Sando, V. Zafiropulos, and W. C. Stwalley, J. Chem. Phys. **92**, 5801 (1990).
[12] P. Kowalczyk and N. Sadeghi, J. Chem. Phys. **102**, 8321 (1995).
[13] H. Katô and C. Noda, J. Chem. Phys. **73**, 4940 (1980).
[14] A. J. Ross, C. Effantin, J. d'Incan, and R. F. Barrow, J. Phys. B **19**, 1449 (1986).
[15] H. Sun and J. Huennekens, J. Chem. Phys. **97**, 4714 (1992).
[16] J. Derouard and N. Sadeghi, J. Chem. Phys. **88**, 2891 (1988).
[17] P. Kowalczyk, J. Chem. Phys. **91**, 2779 (1989).
[18] P. Kowalczyk, J. Derouard, and N. Sadeghi, J. Mol. Spectrosc. **151**, 303 (1992).
[19] M. Baba, S. Tanaka, and H. Katô, J. Chem. Phys. **89**, 7049 (1988).
[20] H. Katô, M. Sakano, N. Yoshie, M. Baba, and K. Ishikawa, J. Chem. Phys. **93**, 2228 (1990).
[21] S. Kasahara, M. Baba, and H. Katô, J. Chem. Phys. **94**, 7713 (1991).
[22] M. Baba, K. Nishizawa, N. Yoshie, K. Ishikawa, and H. Katô, J. Chem. Phys. **96**, 955 (1992).
[23] K. Ishikawa, T. Kumauchi, M. Baba, and H. Katô, J. Chem. Phys. **96**, 6423 (1992).
[24] H. Lefebvre-Brion and R. W. Field, *Perturbations in the Spectra of Diatomic Molecules* (Academic, New York, London, 1986).
[25] W. M. Kosman and J. Hinze, J. Mol. Spectrosc. **56**, 93 (1975); C. R. Vidal and H. Scheingraber, *ibid*. **65**, 46 (1977).
[26] A. Krou-Adohi and S. Giraud-Cotton, J. Mol. Spectrosc. **190**, 171 (1998).
[27] A. V. Abarenov and A. V. Stolyarov, J. Phys. B **23**, 2419 (1990).
[28] Ch. Teichteil, M. Pelissier, and F. Spiegelmann, Chem. Phys. **81**, 273 (1983).
[29] A. Zaitsevskii, Ch. Teichteil, J. Vigué, and G. Bazalgette, Chem. Phys. Lett. **307**, 277 (1999).
[30] L. F. Pacios and P. A. Christiansen, J. Chem. Phys. **82**, 2664 (1985).
[31] M. M. Hurley, L. F. Pacios, P. A. Christiansen, R. B. Ross, and W. C. Ermler, J. Chem. Phys. **84**, 6840 (1986).
[32] A. Zaitsevskii and J. P. Malrieu, Theor. Chem. Acc. **96**, 269 (1997).
[33] A. Zaitsevskii and R. Cimiraglia, Int. J. Quantum Chem. **73**, 395 (1999).
[34] P. Kowalczyk, see AIP document No. PAPS JCPSA-91-2779-43 for line positions of the NaK B-*X*, *c*-X and *b*-X band systems. Order by PAPS number and journal reference from American Institute of Physics, Physics Auxiliary Publication Service, Suite 1N01, 2 Huntington Quadrangle, Melville, NY 11747-4502. Fax: 516-576-2404, Email: paps@aip.org. The price is $1.50 for each microfiche (98 pages) or $5.00 for photocopies of up to 30 pages, and $0.15 for each additional page over 30 pages. Airmail additional. Make checks payable to the American Institute of Physics in U.S. dollars. For additional information on EPAPS (electronic submission), please visit our website http://www.aip.org/pubservs/epaps.html
[35] H. Katô, Bull. Chem. Soc. Jpn. **66**, 3203 (1993).
[36] E. A. Pazyuk, A. V. Stolyarov, I. V. Ushakov, and R. S. Ferber, J. Quant. Spectrosc. Radiat. Transf. **53**, 565 (1995).
[37] Ya. A. Harya, R. S. Ferber, N. E. Kuz'menko, O. A. Shmit, and A. V. Stolyarov, J. Mol. Spectrosc. **125**, 1 (1987).
[38] C. L. Pekeris, Phys. Rev. **45**, 98 (1934).
[39] J. N. Huffaker, J. Chem. Phys. **64**, 3175 (1976).
[40] J. Tellinghuisen, Chem. Phys. Lett. **105**, 241 (1984); A. V. Stolyarov and V. I. Pupyshev, Phys. Rev. A **49**, 1693 (1994); E. A. Pazyuk, A. V. Stolyarov, and V. I. Pupyshev, Chem. Phys. Lett. **228**, 219 (1994).
[41] J. Derouard, H. Debontride, T. D. Nguyen, and N. Sadeghi, J. Chem. Phys. **90**, 5936 (1989).